

Cross Validation in Stochastic Analytic Continuation

Gabe Schumm,^{1,*} Sibin Yang,¹ and Anders W. Sandvik^{1,†}

¹*Department of Physics, Boston University, 590 Commonwealth Avenue, Boston, Massachusetts 02215, USA*

(Dated: June 12, 2024)

Stochastic Analytic Continuation (SAC) of Quantum Monte Carlo (QMC) imaginary-time correlation function data is a valuable tool in connecting many-body models to experiments. Recent developments of the SAC method have allowed for spectral functions with sharp features, e.g. narrow peaks and divergent edges, to be resolved with unprecedented fidelity. Often times, it is not known what exact sharp features are present *a priori*, and, due to the ill-posed nature of the analytic continuation problem, multiple spectral representations may be acceptable. In this work, we borrow from the machine learning and statistics literature and implement a cross validation technique to provide an unbiased method to identify the most likely spectrum. We show examples using imaginary-time data generated by QMC simulations and synthetic data generated from artificial spectra. Our procedure, which can be considered a form of “model selection,” can be applied to a variety of numerical analytic continuation methods, beyond just SAC.

I. INTRODUCTION

Dynamic response functions (spectral functions) provide a key link between the quantum Monte Carlo (QMC) simulations of many-body systems and their experimental counterparts. While it is intractable to measure these spectral function directly, one can instead perform numerical analytic continuation of imaginary-time correlation functions to real frequency. However, this process is what is considered an “ill-posed” problem, meaning that there may be many viable solutions for the spectral function fitting a set of QMC generated data. The Maximum Entropy method (MEM) [1] has been the traditional tool used to tackle this problem and has produced many important results [2]. However, MEM has its limitations, being able only to reproduce broad spectral features, unless prior information about more complicated structure is provided to the algorithm.

An alternative approach to MEM is to instead rely on the stochastic averaging of many solutions for the spectral function that fit the QMC data well. The Stochastic Analytic Continuation (SAC) method [3–15], also referred to as the average spectrum method, achieves this by regularizing the average spectra using a fictitious temperature, Θ , which mediates the competition between the minimization of the goodness-of-fit χ^2 with respect to the QMC data and the favoring of spectra with the high configurational entropy. It is now known that this procedure is equivalent to the MEM when the number of sampled degrees of freedom of the spectrum is large and when the two resulting spectra are compared at the same χ^2 value (although the definition of the entropy may need to be adjusted depending on what degrees of freedom are sampled) [5, 14, 15]. Recent developments in the SAC method have also allowed for the resolution of spectra with sharp features, such as narrow quasi-particle peaks

and edges with power-law singularities, by imposing constraints on the sampling space of the spectral function [10, 14].

In both the plain, “unconstrained” version of SAC, and the newly developed “constrained” SAC sampling schemes, the average χ^2 of the sampled spectra is used to optimize various parameters and gauge the ability of the spectral representation to describe the data. While these methods that rely on the average χ^2 alone have been shown to produce reliable and consistent results, the goal of this study is to provide further confirmation for these simple schemes by taking advantage of concepts from the machine learning and statistics literature. We do this by implementing a cross validation procedure [16, 17].

Cross validation is a tool used to compare how well different models describe a set of data. This is generally achieved by splitting the data into mutually exclusive sets, a training, or sampling, set and a series of testing, or validation, sets. A model is trained on the sampling set, typically by optimizing some type of loss function. After training, the ability of the optimized model to describe the validation data sets is determined using this same loss function. This can provide information about the suitability of the model to describe the data, as well as the level of over-fitting to noise in the sampling data set.

Cross validation has a natural extension to SAC. The imaginary-time correlation function data, calculated using QMC simulations, is typically stored as individual bins, which can be split up into sampling and validation sets. Here, the goodness-of-fit χ^2 is used as the loss function to “train” and to “validate” the resulting spectral function. The concept of using cross validation within SAC was first implemented by Efremkin et al. [18], whose work we draw on and significantly expand upon. Here, we perform an exhaustive study using both synthetic and real QMC data.

In Sec. II we describe the SAC procedure generally, and in Sec. III we explain our crossvalidation scheme in detail. In Sec. IV A and IV B we implement cross validation using the unconstrained SAC method and demonstrate how it is used to determine the optimal sampling tem-

* gschumm@bu.edu

† sandvik@bu.edu

perature, which we compare to the simple criterion previously proposed by Ref. [14]. In Sec. V A and V B, we show how cross validation can be used in practice to determine which SAC sampling parameterization produces the most statistically likely spectrum. In Sec. V A we perform a test using QMC generated data for the $S = 1/2$ antiferromagnetic (AFM) Heisenberg model, where it is known that the spectral function for the $O = S_q^z$ operator contains a power-law divergent edge. In Sec. V B we perform a preliminary test on the $S = 1/2$ AFM Heisenberg model with long-range interactions [19, 20], a model where the exact features of the spectral function are unknown.

II. SAC PROCEDURE

For the purpose of self-containment and to set the notation, we will first provide a brief overview of the SAC procedure, as well as the small adjustments needed for cross validation.

We consider the imaginary-time correlation function of a bosonic operator O at inverse temperature $1/T = \beta$, evaluated at time points $\tau \in [0, \beta/2]$,

$$G(\tau) = \langle O^\dagger(\tau)O(0) \rangle. \quad (1)$$

Here, the imaginary-time dependence is defined in the Heisenberg picture, taking $\hbar = 1$,

$$O(\tau) = e^{\tau H} O e^{-\tau H}. \quad (2)$$

The corresponding spectral function can be defined in terms of the eigenstates $|n\rangle$ of the Hamiltonian H describing the system,

$$S(\omega) = \frac{\pi}{Z} \sum_{m,n} e^{-\beta E_n} |\langle m|O|n\rangle|^2 \delta(\omega - [E_m - E_n]), \quad (3)$$

where Z is the partition function. The relationship between $S(\omega)$ and $G(\tau)$ is given by the equation

$$G(\tau) = \int_0^\infty d\omega S(\omega) K(\tau, \omega), \quad (4)$$

where the bosonic kernel $K(\tau, \omega)$ is defined as

$$K(\tau, \omega) = \frac{1}{\pi} \left(e^{-\tau\omega} + e^{-(\beta-\tau)\omega} \right). \quad (5)$$

For the cross validation procedure, we consider N_B bins of imaginary-time correlation function data evaluated at a set of N_τ points τ_i , $\{G^b(\tau_i)\}$, where $b = 1, 2, \dots, N_B$ and $i = 1, 2, \dots, N_\tau$. The N_B bins are then split into $K + 1$ mutually exclusive sets of equal length $N_k = N_B / (K + 1)$, $\{G^b(\tau_i)\}_k$. For a single cross validation run, one of the $K + 1$ groups will act as the sampling data set, while the other K groups will be used for cross validation. For each group, we compute the average

$$\bar{G}_k(\tau_i) = \frac{1}{N_k} \sum_{b \in k} G^b(\tau_i). \quad (6)$$

Because the statistical errors of different τ points are correlated, the full characterization of the error, and thus the calculation of χ^2 , requires the covariance matrix [1]. We use the bootstrap method to calculate the covariance matrices for each set,

$$C_k^{ij} = \frac{1}{M} \sum_{m=1}^M (G_k^m(\tau_i) - \bar{G}_k(\tau_i))(G_k^m(\tau_j) - \bar{G}_k(\tau_j)) \quad (7)$$

where $G_k^m(\tau_i)$ is the average of a bootstrap sample of N_k randomly chosen bins among the N_k bins in the k th data set, and M is the total number of bootstrap samples, typically much larger than N_B .

Given $S(\omega)$, the corresponding $G(\tau_i)$ values are computed according to Eq. (4) and the χ^2 with respect to the QMC data is given by

$$\chi_k^2 = \sum_{i,j}^{N_\tau} [G(\tau_i) - \bar{G}_k(\tau_i)] [C_k^{-1}]^{ij} [G(\tau_j) - \bar{G}_k(\tau_j)]. \quad (8)$$

Alternatively, one can compute χ_k^2 is the eigenbasis of the covariance matrix:

$$\chi_k^2 = \sum_{i=1}^{N_\tau} \left(\frac{G(\tau_i) - \bar{G}_k(\tau_i)}{\sigma_k(\tau_i)} \right)^2, \quad (9)$$

where $(\sigma_k(\tau_i))^2$ are the eigenvalues of the covariance matrix (and both $G(\tau_i)$ and \bar{G}_k are now computed in this eigenbasis).

In a SAC run, the spectra $S(\omega)$ are importance sampled with a weight

$$P(S) \propto \exp\left(-\frac{\chi^2(S)}{2\Theta}\right). \quad (10)$$

The fictitious temperature Θ is gradually reduced, as in simulated annealing, until a minimum is reached. In the limit $\Theta \rightarrow 0$, the sampled spectrum purely minimizes χ^2 , which will not reproduce the most probable spectrum when noisy data is used. Instead, it has been proposed to use an elevated temperature, which gives the optimal balance of entropy and goodness-of-fit, corresponding to the value where

$$\langle \chi^2(\Theta) \rangle = \chi_{\min}^2 + a\sigma_{\chi^2} \quad (11)$$

where $\sigma_{\chi^2} = \sqrt{2\chi_{\min}^2}$ is used as a proxy for the standard deviation of the χ^2 distribution that the value of $\langle \chi^2 \rangle$ follows and a is an order one number (typically $a = 1/2$ is used). This criterion, motivated by the properties of the χ^2 distribution, has been shown to produce reliable results, reproducing spectra generated from synthetic QMC $G(\tau)$ data with high fidelity [14].

III. CROSS VALIDATION PROCEDURE

We will now describe the implementation of cross validation within the SAC framework laid out above. Using

the $k = 0$ th set of bins as the sampling data set, we carry out a simulated annealing run, as described above. Along with the sampling χ^2 , at each temperature we use the sets $k = 1, \dots, K$ to compute the validation χ^2 value:

$$\chi_{\text{val}}^2 = \frac{1}{K} \sum_{k=1}^K \sum_{i=1}^{N_\tau} \left(\frac{G(\tau_i) - \bar{G}_k(\tau_i)}{\sigma_k(\tau_i)} \right)^2. \quad (12)$$

If we denote the exact correlation function by $G_{\text{ex}}(\tau)$, Eq. (12) can be rewritten as

$$\chi_{\text{val}}^2 = \frac{1}{K} \sum_{k=1}^K \sum_{i=1}^{N_\tau} \left(\frac{G(\tau_i) - G_{\text{ex}}(\tau_i) + G_{\text{ex}}(\tau_i) - \bar{G}_k(\tau_i)}{\sigma_k(\tau_i)} \right)^2, \quad (13)$$

which factors into three terms:

$$\chi_{\text{val}}^2 = X_1 + X_2 + X_3, \quad (14)$$

where

$$X_1 = \frac{1}{K} \sum_{k=1}^K \sum_{i=1}^{N_\tau} \left(\frac{G(\tau_i) - G_{\text{ex}}(\tau_i)}{\sigma_k(\tau_i)} \right)^2, \quad (15a)$$

$$X_2 = \frac{1}{K} \sum_{k=1}^K \sum_{i=1}^{N_\tau} \left(\frac{\bar{G}_k(\tau_i) - G_{\text{ex}}(\tau_i)}{\sigma_k(\tau_i)} \right)^2, \quad (15b)$$

$$X_3 = \frac{1}{K} \sum_{k=1}^K \sum_{i=1}^{N_\tau} \frac{2(\bar{G}_k(\tau_i) - G_{\text{ex}}(\tau_i))(G_{\text{ex}}(\tau_i) - G(\tau_i))}{\sigma_k^2(\tau_i)}. \quad (15c)$$

Here, X_1 contains purely information about how well the estimated $G(\tau)$, calculated from the sampled $S(\omega)$, describes the exact correlation function. This will vary as we change Θ , or any other parameter used in the SAC program, and will be minimized by the most statistically likely spectral function, given input data $\bar{G}_0(\tau)$ and C_0^{ij} .

X_2 is the the χ^2 value for the validation data with respect to the underlying data G_{ex} , averaged over each of the K validation data sets. The value of X_2 will follow the χ^2 distribution with $N_{\text{dof}} = N_\tau$, and will have a mean of $E[X_2] = N_{\text{dof}} = N_\tau$ and a variance of $V[X_2] = 2N_{\text{dof}} = 2N_\tau$. This term is independent of any SAC parameter and will simply contribute a background value of N_τ , in the limit of large K .

X_3 contains both information about the accuracy of $G(\tau)$ with respect to $G_{\text{ex}}(\tau)$ and the deviation of the $\bar{G}_k(\tau)$ with respect to $G_{\text{ex}}(\tau)$. However, we expect that fluctuations of $\bar{G}_k(\tau)$ will follow a Gaussian distribution with a mean of zero, so in the limit of large K , this term should also have a mean of zero. While, X_3 does depend on the SAC parameters (e.g. Θ), as well as on the covariance of each validation data set, we have found that the dominant contribution is indeed from the Gaussian fluctuations of $\bar{G}_k(\tau)$, so this term can be approximated as zero when K is large.

Using the above properties, the *reduced* validation χ^2 becomes simply

$$\chi_{\text{val}}^2/N_\tau \approx \frac{1}{K} \sum_{k=1}^K \sum_{i=1}^{N_\tau} \left(\frac{G(\tau_i) - G_{\text{ex}}(\tau_i)}{\sigma_k(\tau_i)} \right)^2 + 1. \quad (16)$$

IV. OPTIMAL SAMPLING TEMPERATURE

A. Single Gaussian Spectrum

Our first implementation of cross validation will be to provide support for the optimal Θ criterion, Eq. (11). The motivation behind this criterion is to place the simulation in a temperature range safely above the regime of over-fitting, which we will be able to identify by tracking the behavior of the validation χ^2 as Θ is lowered.

For our tests, we will use synthetic $G(\tau)$ data aimed to mimic the data from a QMC simulation. Given an artificial spectrum $S(\omega)$, we use Eq. (4) to calculate the exact imaginary-time correlation function. To introduce the statistical errors necessarily present in QMC data, we generate many $G(\tau)$ bins with noise that is correlated in imaginary-time. This is done by first generating normally distributed noise for each τ point $\sigma_0(\tau_i)$, and then taking the weighted averaging over all τ points with an exponentially decaying weight function:

$$\sigma(\tau_i) = \sum_{j=1}^{N_\tau} \sigma_0(\tau_j) e^{-|\tau_i - \tau_j|}. \quad (17)$$

It was shown that the presence of covariance in the data actually improves the results of the SAC method [14], so including this in our synthetic data is critical when comparing to QMC data.

We use a spectrum consisting of a single Gaussian peak, centered at $\omega = 3$ and with a width $\sigma = 0.5$. This spectrum can be essentially perfectly reproduced using the unconstrained SAC procedure. Here, $S(\omega)$ is represented as a weighted sum of δ -functions that can freely move around in frequency-space,

$$S(\omega) = \sum_i A_i \delta(\omega - \omega_i). \quad (18)$$

In this example, we use $N_\omega = 5,000$ total δ -functions, which is large enough to no longer detect and dependence of $S(\omega)$ on N_ω .

We generate $K = 20$ independent validation data sets, each containing 1000 bins of synthetic $G(\tau)$ data. While it is certainly reasonable to generate this volume of data using modern QMC methods, this would be an inefficient use of computational resources given that the majority of the data is being used for validation. However, we use this large quantity so that the simplifications made in the large K limit are more accurately realized. As we show in Sec. V A, one can still use cross validation with far fewer $G(\tau)$ bins, even when this limit is not fully reached.

When converting from $S(\omega)$ to $G(\tau)$, we set the inverse temperature $\beta = 2$ and use a τ spacing of $\Delta_\tau = 0.0625$, giving $N_\tau = 16$ imaginary time points. The relatively low value of β used here was chosen in light of the fact that spectra consisting of broad and smooth features, such as the simple Gaussian used here, would usually be found at higher temperatures. We generate synthetic data from

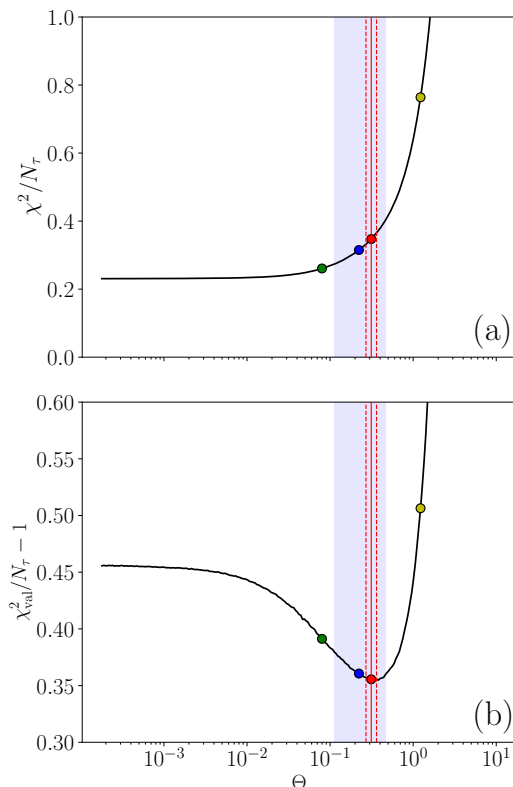


FIG. 1. For the spectral function shown in Fig. 2, the average of $K = 20$ cross validation annealing runs using synthetic data with a noise level of $\sigma = 10^{-5}$. Panels (a) and (b) show the behavior χ^2 and χ_{val}^2 versus Θ . The temperature range corresponding to Eq. (11) with $a = 0.25 - 1.0$ is shaded in blue. The temperature where χ_{val}^2 is at its minimum is marked by a red vertical line. The spread (one standard deviation) in the location of the χ_{val}^2 minimum is denoted by the red dashed lines. The χ^2 and χ_{val}^2 values have been normalized by the number of τ points, and the background value of 1, corresponding to X_2 in Eq. (14) has been subtracted from χ_{val}^2 . The colored points along the curves mark the sampling temperatures of the corresponding spectra in Fig. 2

this spectrum with an error level $\sigma = 10^{-5}$, where the error level is defined as the magnitude of the error bar on the averaged correlation function, $\bar{G}_k(\tau_i)$, for the largest τ point included, when normalized so that $G_k(0) = 1$. For larger β , a cutoff is typically introduced at the τ value where the relative error on $G(\tau)$ is greater than 10%, which we instead use to quantify the error level.

The results of the cross validation procedure are shown in Fig. 1 and Fig. 2. Fig. 1 show the behavior of χ^2 (panel (a)) and χ_{val}^2 (panel (b)) versus Θ , averaged over all $K = 20$ validation data sets. The temperature range corresponding to Eq. (11) with $a = 0.25 - 1.0$ is shaded in blue. The temperature where χ_{val}^2 is at its minimum is marked by a red vertical line, with the red dashed lines denoting the standard deviation of the location of the minimum. In practice, it is useful to repeat this process, rotating which of the $K + 1$ data sets is used for sampling

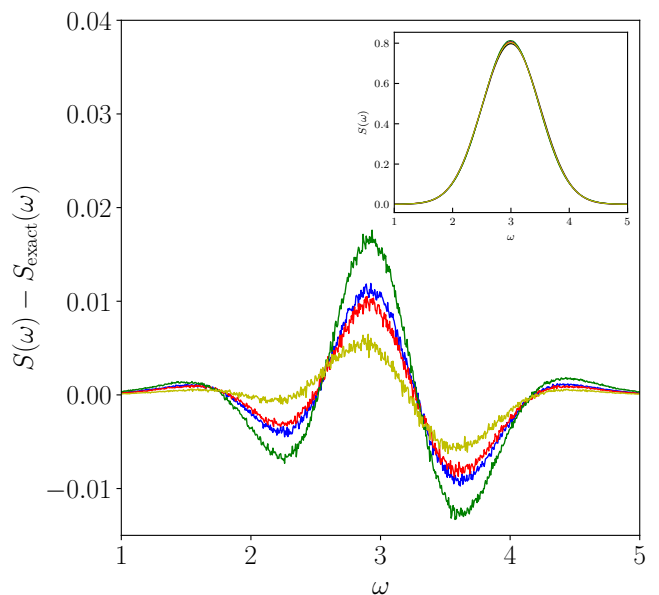


FIG. 2. Deviation between the exact spectrum and those sampled at four different temperatures: the temperature where $a = 0.5$ (blue), the temperature where χ_{val}^2 is minimized (red), and temperatures above/below (yellow/green) this minimum. Inset: the spectral function themselves. In this case, it is difficult to distinguish the different spectra, as they nearly overlap.

and which are used for validation, averaging the results in the end. However, for this test we found this was not necessary given the large number of synthetic data bins that can be easily generated.

In Fig. 2, we show the difference between the the exact spectrum and the SAC spectra sampled at the temperature where $a = 0.5$ (blue), at the χ_{val}^2 minimum (red), and at temperatures above (yellow) and below (green) the validation minimum, for comparison. In the inset of Fig. 2, we show the spectral functions themselves. To generate these spectra we ran the SAC procedure using all bins, recombined from the $K + 1 = 21$ sets, thus taking full advantage of the data at hand.

In this case, the minimum of χ_{val}^2 is quite sharp, and agrees very well with the temperature from Eq. (11). Consequently, the red and blue spectra in Fig. 1 are nearly identical, and, for all intents and purposes, are equally valid representations of the true spectrum, shown in black. The green and yellow spectra are included to show the relatively small Θ dependence for this simple spectrum.

B. Double Gaussian Spectrum

We now turn to an example where the unconstrained sampling parameterization in Eq. (18) cannot reproduce the artificial spectrum quite as closely. The spectrum we consider is composed of a pair of Gaussian peaks, one

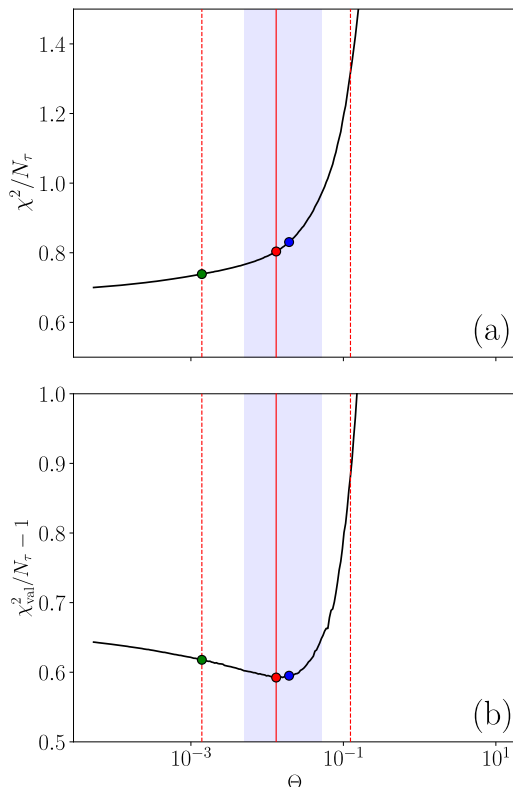


FIG. 3. For the spectral function shown in Fig. 4, the average of $K = 40$ cross validation annealing runs using the synthetic data with a noise level of $\sigma = 10^{-5}$. Panels, symbols, and set up are the same as in Fig. 1.

broader than the other, that intersect slightly. The area near the sharp dip, where the two peaks intersect, poses difficulties and would require a lower error level than one could reasonably achieve using real QMC data to fully resolve [14]. As such, the criterion in Eq. (11) provides an estimate for the temperature corresponding to the best possible spectrum, given these limitations.

We preform the same test as in Sec. IV A, and present the results in Fig. 3. In this case, both the validation minimum and the temperature range corresponding to the criterion with a ranging from 0.25 and 1 are much broader, but still align quite well with one another. The higher level of uncertainty is a reflection of the inability of the unconstrained sampling scheme to reproduce this spectrum nearly as well as in the previous case, which can be seen clearly in Fig. 4. Here we again plot the spectra at the validation χ^2 minimum (red) and at the temperature where $a = 0.5$ (blue), as well as at a slightly lower temperature, corresponding to one standard deviation away from the validation minimum (green). It is interesting to note that, at the lower sampling temperature, SAC is able to reproduce certain features of the exact spectrum better than at the temperatures corresponding to the validation minimum or $a = 0.5$ (such as the position of the first peak and area where the two peaks intersect), while

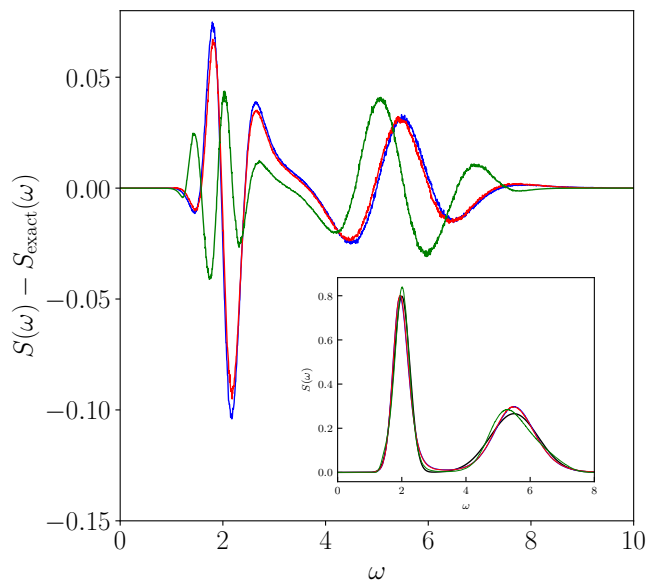


FIG. 4. Deviation between the extra spectrum and those sampled at three different temperatures: the temperature where $a = 0.5$ (blue), the temperature where χ^2_{val} is minimized (red), and at a slightly lower temperature, corresponding to one standard deviations below this minimum (green). We note that the magnitude of the deviation is both a reflection of the error in the amplitudes and the locations of the two Gaussian peaks. Inset: the spectral function themselves. Just as in Fig. 2, the red and blue spectra are nearly indistinguishable.

reproducing others not as well (such as the position of the second peak). This is consistent with the broadness of the validation χ^2 minimum, as it is not necessarily clear which is the better choice of spectra.

We emphasize that using cross validation to determine the optimal sampling temperature is not necessary when running SAC with real QMC data. Rather, these test-cases show that the criterion in Eq. (11) indeed samples safely above the regime of over-fitting, while still keeping the χ^2 at an acceptable level, and *should* be used as the method of fixing Θ in real use-cases. In the following sections we will explore a more practical and decisive use for our cross validation procedure.

V. OPTIMAL SPECTRAL PARAMETERIZATION

A. Heisenberg Chain

Our second application of cross validation will be to help determine which SAC sampling parameterization to use when the exact spectral features are unknown. In Eq. (18), we model the spectrum as unconstrained δ -functions with variable amplitudes and positions. However, if certain restrictions are imposed on the locations and amplitudes of the δ -function, the SAC method is

able to reproduce sharp spectral features present only at low temperature, such as narrow quasi-particle peaks and power-law edge singularities [10, 14, 21]. We call this class of SAC sampling schemes “constrained.”

A spectrum containing a dominate δ -peak followed by a smooth continuum can be reproduced using the parameterization

$$S_{\text{peak}}(\omega) = A_0\delta(\omega - \omega_0) + \sum_i A_i\delta(\omega - \omega_i), \quad (19)$$

where $A_0 + \sum_i A_i = 1$ and the constraint $\omega_i > \omega_0$ for all i is imposed during the sampling process. With this parameterization, the location of the peak, ω_0 , is sampled within the program, along with all of the other δ -functions, but the weight of the dominant δ peak, A_0 , is fixed and optimized using a simple scan to find a χ^2 minimum, as detailed in Ref. [14]. This type of spectral function is appropriate for describing the spectrum of the $S = 1/2$ AFM Heisenberg model in two-dimensions (2D) [22], where linear spin-wave theory predicts the presence of a dominant, “single-magnon” peak [23], while an incoherent continuum at higher energy can be attributed to either multimagnon excitations or partially deconfined spinon excitations, both of which cannot be captured by convention spin-wave theory [21]. The parameterization of SAC in Eq. (19) has been used to produce results for the spectral function of the aforementioned square-lattice Heisenberg model that agreed very well with results from inelastic neutron-scattering experiments on a material considered the best physical realization of this model [21].

Another example of a sharp spectral feature that can only be resolved using a constrained SAC sampling parameterization is an edge singularity. In quantum many-body systems with fractionalized excitations, spectral weight may be spread over a range of energies, often with a power-law distribution that diverges at some frequency ω_q , where q is the total momentum of the fractionalized quasiparticle [14]. One of the most well know examples of this is the spectral function of the operator $O = S_q^z(\omega)$ in the $S = 1/2$ AFM Heisenberg chain. Using the Bethe ansatz (BA) solution, it was shown that in the thermodynamic limit, this spectral function diverges as $(\omega - \omega_q)^{-1/2}$, with a logarithmic correction [24–26].

A spectrum with this type of feature can be realized in SAC by restricting the locations of the sampled δ -functions such that the distance between adjacent δ 's monotonically increases [10, 14]:

$$S_{\text{edge}}(\omega) = \sum_i A_i\delta(\omega - \omega_i), \quad (20)$$

with the constraint $\omega_{i+1} - \omega_i > \omega_i - \omega_{i-1}$, i.e. monotonically increasing spacing. Due to entropic pressure, this parameterization naturally produces a spectrum where the mean density of the δ -functions forms precisely an edge singularity with the asymptotic behavior $(\omega - \omega_q)^{-1/2}$. Away from this edge, the data instead dictates the exact shape of the spectrum. It also possible to

resolve an edge diverging with any power p , that can be optimized with a scan, by properly adjusting the amplitudes A_i , as detailed in Ref. [14], but in these tests we just consider the $p = 1/2$ case.

In most cases, the exact features of the true spectral function are not known, and one must test out these various parameterizations. However, relying on the value of χ^2 alone to compare the resulting spectra is not always reliable, since the SAC method can produce spectra with an acceptable χ^2 values even when the improper parameterization is being used (a consequence of the “ill-posed” problem). Our cross validation procedure can be used as an unbiased method to determine which parameterization is best amongst the group of parameterizations considered, i.e. for “model selection” [17].

We demonstrate the ability to discriminate between models using real QMC data, generated using the stochastic series expansion (SSE) method [27], for the $S = 1/2$ AFM Heisenberg chain. We follow the procedure outlined in Sec. III, again with $K = 20$ validation sets with an error level of $\sigma \sim 10^{-5}$. The system size used here is $L = 512$, and the QMC simulation was run using the inverse temperature $\beta = 1024$, which is large enough to access ground state properties. While the predicted power-law form holds for all momenta q in $S_q^z(\omega)$, we consider just $q = \pi/2$, as a test case.

For this test, we repeat the cross validation process, rotating which of the $K + 1 = 21$ sets of QMC data is used for sampling, and which ones are used for validation, which we found was necessary given the quality and quantity of the QMC-generated data. The final result is the average over all of the rotations, which we use to compare each of the three parameterizations.

Fig. 5 shows the sampling (panel (a)) and validation (panel (b)) χ^2 values versus Θ for each parameterization: unconstrained (red), single-peak (blue), and edge (green). Here, we normalize by the number of τ points (in this case 50, with $\Delta_\tau = 0.1$) and subtract one from the normalized validation χ^2 to account for the background contribution, X_2 in Eq. (14). Because the entropy contents of the spectra defined with each parameterizations are different, the annealing paths they each take differ, so it is also informative to compare the validation χ^2 values at the same value of the sampling χ^2 . This is done in panel (c), where we plot the validation χ^2 versus the sampling χ^2 throughout the annealing runs.

While it is difficult to glean any information about the relative performance of the three parameterizations from the sampling χ^2 , the validation χ^2 paints a much different picture. At each temperature, the the edge parameterization has the lowest validation χ^2 , followed by the single peak case, and then unconstrained sampling. This would suggest that the edge is indeed the most appropriate parameterization, in agreement with the BA solution for this model. This conclusion can also be made when comparing the values of χ_{val}^2 at fixed χ^2 , panel (c). Here, the single peak and edge parameterizations perform equally as well up until the normalized sampling χ^2

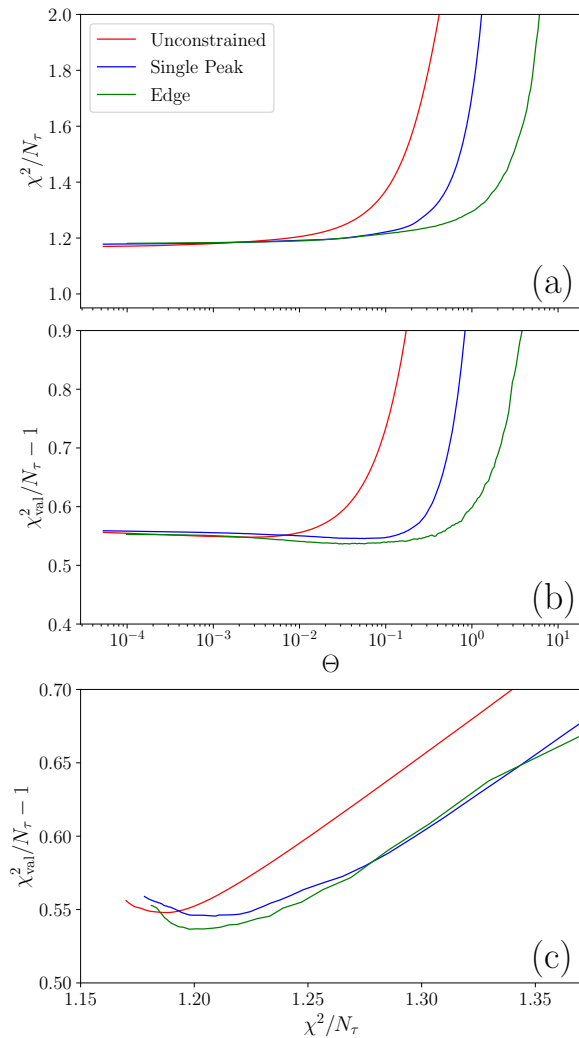


FIG. 5. Cross validation results for $S(q = \pi/2, \omega)$ of the $S = 1/2$ Heisenberg chain ($L = 512$, $\beta = 1024$). The sampling (a) and validation (b) χ^2 values, normalized by the number of τ points, are averaged over all rotations of the sampling and validation data sets (twenty in total). In panel (c), we plot the validation χ^2 as a function of the sampling χ^2 , to compare the three parameterizations at fixed sampling χ^2 values.

reaches ~ 1.27 , at which point the validation χ^2 curve for the edge parameterizations dips below that of the single peak. The χ^2 values corresponding to the criterion in Eq (11) with $a = 0.5$ are 1.26, 1.30 and 1.30 for the unconstrained, peak, and edge parameterization, respectively, which are the values for the spectra in Fig. 6. We note, however, that the spectra do not change significantly when sampled at slightly lower temperatures, corresponding to the minima of each χ^2_{val} curve, just as in Sec. IV A. We conclude that it is thus important take into consideration both the minimum value of each χ^2_{val} curve and the path the curves take when making these comparisons.

We now compare the corresponding spectra, shown in

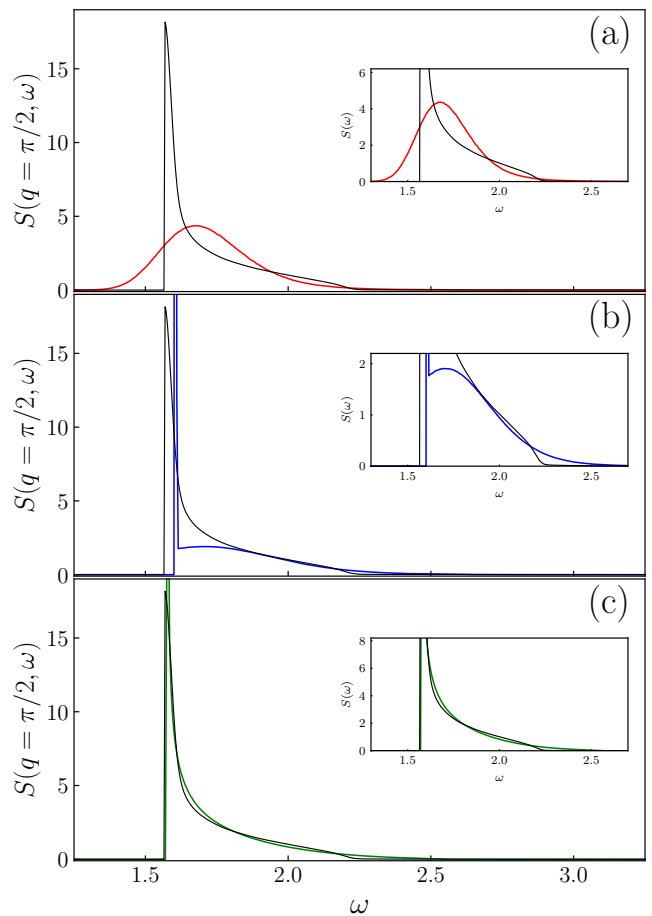


FIG. 6. Spectra corresponding to the three parameterizations in Fig. 5, unconstrained (a), single-peak with $A_0 = 0.50$ (b), and edge (c). For each parameterization, the spectra are sampled at the temperatures corresponding to the criterion in Eq. (11), using their respective sampling χ^2 curves. For the unconstrained sampling parameterization, we use $N\omega = 2,000$ δ -functions. For the single-peak parameterization we use a $N_p = 1$ leading δ -function with a relative weight of $A_0 = 0.5$ and $N_c = 2,000$ continuum δ -functions. For the edge parameterization, we use $N_\omega = 320$ δ -functions. In each panel, we also plot the BA results (black curves), which have also been subject to smoothing [28], resulting in more rounded peaks. Insets: same spectra, but on zoomed in scales.

Fig. 6, to see if the hierarchy suggested by the validation χ^2 is borne out in the results of the analytic continuation process. As reflected by the relative differences between the χ^2_{val} curves, the single-peak and edge spectra share similar features, such as a lower bound near $\omega = 1.5$, while the unconstrained sampling produces a spectra with considerable spectral weight below this edge. The BA result [28], shown in black, agrees very well with the edge spectra (with edges that nearly perfectly align), moderately well for the peak spectra (but with some glaring deviations), and very poorly with the unconstrained spectra, further supporting the results of our cross validation test. Here, it should be noted that the BA spectrum

has been subject to significant broadening, and furthermore, the calculation of this spectrum only took into consideration two-spinon and four-spinon contributions. As such, it is known that a few percent of the total spectral weight is missing, which could at least partially explain the deviations in the tail in Fig. 6(c).

While it is encouraging that in this test the edge parameterization beats out the unconstrained and single-peak, the difference between the validation χ^2 's is likely too small to claim with any certainty that the spectrum truly contains this feature. Furthermore, for a chain of length 512, the exact $T = 0$ spectrum likely only contains ~ 100 delta functions with significant weight, deduced by extrapolating from the results for smaller system sizes [29, 30]. With this in mind, it's quite possible that a spectrum composed of a dominant peak plus a smooth continuation is actually the best representation for this finite system, while only in the thermodynamic limit would the edge parameterization truly be the most accurate. Performing more cross validation tests using synthetic spectra, where these sharp features are exactly realized, will be necessary to gauge the reliability of this procedure.

B. Heisenberg Chain with Long-Range Interactions

We now turn to a case where the exact features contained in the spectral function are unknown, the unfrustrated AFM Heisenberg chain with power-law decaying interactions:

$$H = \sum_{r=1}^{L/2} J_r \sum_{i=1}^L \mathbf{S}_i \cdot \mathbf{S}_{i+r}, \quad (21)$$

where

$$J_r = G \frac{(-1)^{r-1}}{r^\alpha}, \quad G = \left(1 + \sum_{r=2}^{L/2} \frac{1}{r^\alpha} \right)^{-1}. \quad (22)$$

Interest in this model is rooted in its possible connection to the 2D square lattice AFM Heisenberg model, as the long-range, staggered interactions allow for symmetry breaking and true long-range order to form in this 1D quantum magnet at $T = 0$, effectively increasing its dimensionality [19]. The excitation spectra of the long-range Heisenberg chain is a key ingredient in understanding the nature of its ground state, and the ability to resolve sharp features with the aforementioned constrained SAC sampling schemes may help clear up the long-standing uncertainties surrounding this model. An extensive study of this system will be published in a separate paper, where spectral functions are calculated in both the Néel ordered phase ($\alpha < \alpha_c = 2.22(1)$), as well as in the quasi long-range ordered (QLRO) phase ($\alpha > \alpha_c$) [20].

The Néel phase provides an excellent application for cross validation, because of the uncertainty surrounding

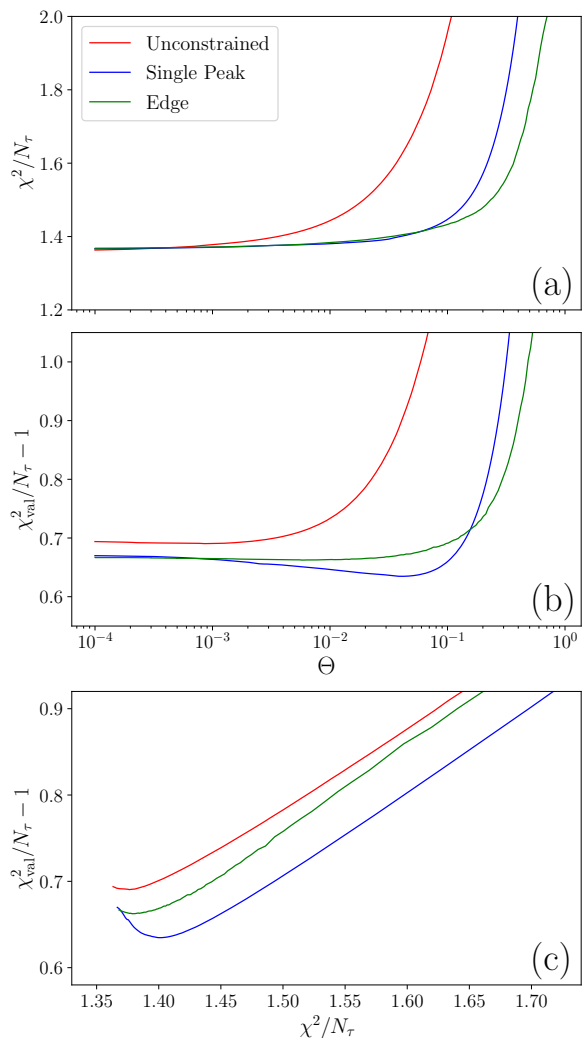


FIG. 7. Cross validation results for the $S = 1/2$ Heisenberg chain with long-range interactions ($L = 256$, $\beta = 256$), for $\alpha = 2.0$. Panels and set up are the same as in Fig. 5.

the nature of the ground state excitations. In the QLRO regime, it is expected that the spectral functions contains a power-law edge, in light of the BA results discussed in Sec. VB. A previous study on a Heisenberg chain with similar long-range interactions focused only on resolving spectral functions with sharp magnon peaks when the system is in Néel phase [19]. This study used the time-dependent Density Matrix Renormalization Group (tDMRG) method, which is known to produce artificially broadened peaks due to limits on the width of the real-time window used in the calculations. The δ -function peak SAC parameterization could potentially provide a significant improvement to these results.

It is also possible that on the Néel side of the quantum phase transition (QPT) the spectral function contains a power-law edge, something that has not been considered due to the difficulty of resolving this type of structure using traditional analytic continuation meth-

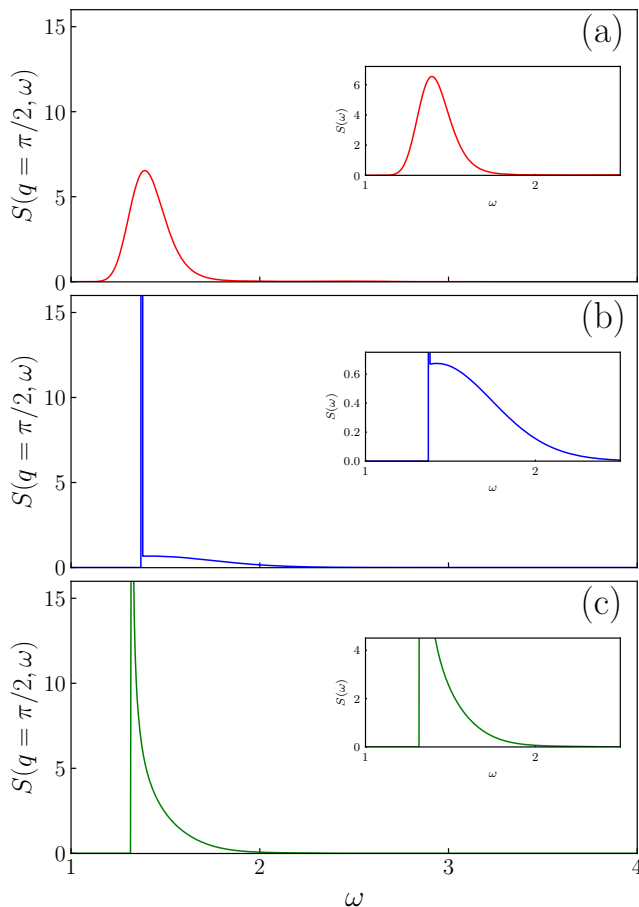


FIG. 8. Spectra corresponding to the three parameterizations in Fig. 7, unconstrained (a), single-peak with $A_0 = 0.80$ (b), and edge (c). Panels and set up are the same as in Fig. 6

ods. Here, we analyze results from our auxiliary paper, Ref. [20], using cross validation to test these three SAC parameterizations for $\alpha = 2.0$, in the Néel ordered regime but close to the QPT. In Ref. [20], a broader set of SAC parameterizations are tested, but here, we will only focus on the three discussed thus far.

Figure 7 shows the results of the cross validation procedure for this model. Here, we again use QMC data generated using the SSE method, for a system of length $L = 256$ at inverse temperature $\beta = 256$, and we consider the operator $O = S_{q=\pi/2}^z$. The number of validation data sets used in this run was $K = 20$, which was chosen to limit the error level to $\sigma \sim 10^{-5}$.

The the validation χ^2 curves in Fig. 7(b) suggest that single-peak parameterization now preforms best, followed by the edge parameterization, and then finally unconstrained sampling. This is even clearer when comparing χ_{val}^2 at fixed χ^2 , panel (c). The hierarchy of parameterizations is extremely stable over the entire annealing run, and a large gap separates the single peak parameterization from the other two. We contrast this with Fig. 5(c), where the single peak and edge χ_{val}^2 values are

much closer, and only deviate as they approach their minima.

We can understand the difference in the behavior of the curves in Fig. 5(c) and Fig. 7(c) as a reflection of difference between the applicabilities of these spectral forms for each model. As discussed in Sec. V A, the single peak parameterization performing comparably to the edge parameterization for the plain Heisenberg chain can be explained by finite-size effects; only in the thermodynamic limit would one expect a completely smooth and monotonic spectral function. On the other hand, the long-range Heisenberg chain with $\alpha = 2.0$ exhibits Néel order and will thus host coherent, spin-wave excitations, albeit with anomalous dispersion [20, 31, 32]. We then expect the spectral function to contain a dominant magnon peak, as reproduced by the single peak parameterization. In this case, the elevated χ_{val}^2 for the edge parameterization reflects that a monotonically decaying continuum does not follow this peak; the error contributed by the use of this improper parameterization is systematic. It will be very informative to perform this test for values of $\alpha > \alpha_c$, in the QRLO phase where a power law divergent spectral function is expected instead.

VI. DISCUSSION

We have explored the use of cross validation in the SAC method, as both a confirmation of the optimal Θ criterion, as well as a tool to select the most likely spectral parameterization for a given model. In our test cases using synthetic data, we found excellent agreement between the optimal Θ criterion Eq. (11) and the location of the cross validation minimum. For the more complex of the two test cases, the double-Gaussian, the broad validation χ^2 minimum reflected the difficulties posed by the relatively sharp features contained in this spectrum. In principle this spectrum can be resolved using SAC, but the unconstrained sampling introduces entropic distortions that produce noticeable deviations from the exact result. As a result, all sampling temperatures within the broad minimum produce acceptable representations of the exact spectrum, which we demonstrated by using a Θ value one standard deviation below the average minimum value. Interestingly, at this lower sampling temperature some features of the spectrum were actually reproduced better. Since using cross validation to fix Θ would be a very poor use of computational resources, it is very encouraging that the optimal Θ criterion agrees so well with the the results of the validation procedure.

A promising, and more decisive use of cross validation, is in “model selection.” While the recent developments in the constrained SAC sampling schemes have allowed for the resolution of spectra with sharp features, the ill-posed nature of the analytic continuation problem still presents obstacles for the implementation of these new methods. When many different spectra give acceptable χ^2 values, cross validation is perhaps the least biased way to deter-

mine which parameterizations is most likely. Our results for the $S = 1/2$ AFM Heisenberg chain suggest that cross validation indeed can accomplish this task. Cross validation should be an extremely valuable tool in the study of highly correlated, many-body systems if it can be used to differentiate quantum phases of matter via their spectral features. Further tests on other systems with known spectral features will be very instructive.

The test on the Heisenberg chain with long-range interactions also produced promising results, appearing to correctly identify which side of the QPT the system was on, based on the spectral features alone. While the exact features are only known with certainty in the limiting cases of α , $\alpha \rightarrow 0$ and $\alpha \rightarrow \infty$, it is likely that these features persists throughout either side of the QPT. Further tests at multiple different values of α are still needed, and some will be presented in Ref. [20], but as a general diagnostic tool, cross validation shows much promise in the practice of numerical analytic continuation of QMC data.

Our cross validation scheme is not only applicable to SAC, but can also be applied other numerical analytic continuation methods, such as MEM. Based on our tests,

a promising application of cross validation would be in the selection of the default model used in MEM. While not exactly analogous to the SAC parameterization, there are similarities between these two user-controlled inputs, such as their effects on the shape, and thus entropy, of the output spectra. Often times, perturbation theory is used to select the MEM default model, where some parameter in the perturbative solution is optimized to select the “best” spectra [1]. Cross validation could be used to aide in this optimizations process or to compare entirely different default models, perhaps from different perturbative solutions of the model under consideration.

VII. ACKNOWLEDGEMENTS

We would like to thank Markus Holzmann for useful discussions that inspired this study. This research was supported by the Simons Foundation under Grant No. 511064. The numerical calculations were carried out on the Shared Computing Cluster managed by Boston University’s Research Computing Services.

-
- [1] M. Jarrell and J. Gubernatis, Bayesian inference and the analytic continuation of imaginary-time quantum monte carlo data, *Physics Reports* **269**, 133 (1996).
 - [2] D. Bergeron and A.-M. S. Tremblay, Algorithms for optimized maximum entropy and diagnostic tools for analytic continuation, *Phys. Rev. E* **94**, 023303 (2016).
 - [3] S. R. White, The average spectrum method for the analytic continuation of imaginary-time data, in *Computer Simulation Studies in Condensed Matter Physics III*, edited by D. P. Landau, K. K. Mon, and H.-B. Schüttler (Springer Berlin Heidelberg, Berlin, Heidelberg, 1991) pp. 145–153.
 - [4] A. W. Sandvik, Stochastic method for analytic continuation of quantum monte carlo data, *Phys. Rev. B* **57**, 10287 (1998).
 - [5] K. S. D. Beach, Identifying the maximum entropy method as a special limit of stochastic analytic continuation (2004), arXiv:cond-mat/0403055 [cond-mat.str-el].
 - [6] K. Vafayi and O. Gunnarsson, Analytical continuation of spectral data from imaginary time axis to real frequency axis using statistical sampling, *Phys. Rev. B* **76**, 035115 (2007).
 - [7] D. R. Reichman and E. Rabani, Analytic continuation average spectrum method for quantum liquids, *The Journal of Chemical Physics* **131**, 054502 (2009).
 - [8] O. F. Syljuåsen, Using the average spectrum method to extract dynamics from quantum monte carlo simulations, *Phys. Rev. B* **78**, 174429 (2008).
 - [9] S. Fuchs, T. Pruschke, and M. Jarrell, Analytic continuation of quantum monte carlo data by stochastic analytical inference, *Phys. Rev. E* **81**, 056701 (2010).
 - [10] A. W. Sandvik, Constrained sampling method for analytic continuation, *Phys. Rev. E* **94**, 063308 (2016).
 - [11] Y. Q. Qin, B. Normand, A. W. Sandvik, and Z. Y. Meng, Amplitude mode in three-dimensional dimerized antiferromagnets, *Phys. Rev. Lett.* **118**, 147207 (2017).
 - [12] K. Ghanem and E. Koch, Average spectrum method for analytic continuation: Efficient blocked-mode sampling and dependence on the discretization grid, *Phys. Rev. B* **101**, 085111 (2020).
 - [13] K. Ghanem and E. Koch, Extending the average spectrum method: Grid point sampling and density averaging, *Phys. Rev. B* **102**, 035114 (2020).
 - [14] H. Shao and A. W. Sandvik, Progress on stochastic analytic continuation of quantum monte carlo data, *Phys. Rep.* **1003**, 1 (2023), progress on stochastic analytic continuation of quantum Monte Carlo data.
 - [15] K. Ghanem and E. Koch, Generalized maximum entropy methods as limits of the average spectrum method, *Phys. Rev. B* **108**, L201107 (2023).
 - [16] C. M. Bishop, *Pattern Recognition and Machine Learning (Information Science and Statistics)* (Springer-Verlag, Berlin, Heidelberg, 2006).
 - [17] P. Mehta, M. Bukov, C.-H. Wang, A. G. Day, C. Richardson, C. K. Fisher, and D. J. Schwab, A high-bias, low-variance introduction to machine learning for physicists, *Physics Reports* **810**, 1 (2019), a high-bias, low-variance introduction to Machine Learning for physicists.
 - [18] V. Efremkin, J.-L. Barrat, S. Mossa, and M. Holzmann, Time correlation functions for quantum systems: Validating Bayesian approaches for harmonic oscillators and beyond, *The Journal of Chemical Physics* **155**, 134108 (2021).
 - [19] L. Yang and A. E. Feiguin, From deconfined spinons to coherent magnons in an antiferromagnetic Heisenberg chain with long range interactions, *SciPost Phys.* **10**, 110 (2021).

- [20] S. Yang, G. Schumm, and A. Sandvik, Dynamic structure factor of spin-1/2 chains with long-range interactions (in preparation).
- [21] H. Shao, Y. Q. Qin, S. Capponi, S. Chesi, Z. Y. Meng, and A. W. Sandvik, Nearly deconfined spinon excitations in the square-lattice spin-1/2 heisenberg antiferromagnet, *Phys. Rev. X* **7**, 041072 (2017).
- [22] C. M. Canali and M. Wallin, Spin-spin correlation functions for the square-lattice heisenberg antiferromagnet at zero temperature, *Phys. Rev. B* **48**, 3264 (1993).
- [23] J.-i. Igarashi, $1/s$ expansion for thermodynamic quantities in a two-dimensional heisenberg antiferromagnet at zero temperature, *Phys. Rev. B* **46**, 10763 (1992).
- [24] J.-S. Caux and J. M. Maillet, Computation of dynamical correlation functions of heisenberg chains in a magnetic field, *Phys. Rev. Lett.* **95**, 077201 (2005).
- [25] J.-S. Caux, R. Hagemans, and J. M. Maillet, Computation of dynamical correlation functions of heisenberg chains: the gapless anisotropic regime, *Journal of Statistical Mechanics: Theory and Experiment* **2005**, P09003 (2005).
- [26] R. G. Pereira, J. Sirker, J.-S. Caux, R. Hagemans, J. M. Maillet, S. R. White, and I. Affleck, Dynamical spin structure factor for the anisotropic spin-1/2 heisenberg chain, *Phys. Rev. Lett.* **96**, 257202 (2006).
- [27] A. W. Sandvik, Computational Studies of Quantum Spin Systems, *AIP Conference Proceedings* **1297**, 135 (2010).
- [28] BA results from Ref. [25] provided by J.-S. Caux (private communication).
- [29] L. Wang and H.-Q. Lin, Dynamic structure factor from real time evolution and exact correction vectors with matrix product states (2019), arXiv:1901.07751 [cond-mat.str-el].
- [30] H. D. Xie, R. Z. Huang, X. J. Han, X. Yan, H. H. Zhao, Z. Y. Xie, H. J. Liao, and T. Xiang, Reorthonormalization of chebyshev matrix product states for dynamical correlation functions, *Phys. Rev. B* **97**, 075111 (2018).
- [31] E. Yusuf, A. Joshi, and K. Yang, Spin waves in antiferromagnetic spin chains with long-range interactions, *Phys. Rev. B* **69**, 144412 (2004).
- [32] N. Laflorencie, I. Affleck, and M. Berciu, Critical phenomena and quantum phase transition in long range heisenberg antiferromagnetic chains, *Journal of Statistical Mechanics: Theory and Experiment* **2005**, P12001 (2005).